ACS OMEGA

http://pubs.acs.org/journal/acsodf

Article

Electrostatic Effect on Core−Shell Micro-spheres with Mixed Charges as Adaptive Plugging Agents for Enhanced Oil Recovery

Hui Xu, Zhiqing Su, Yingcheng Li,* Guang Yang, Xue Pu, Hui Sun, Jun Jin, and Yanmin Xia

Cite This: *ACS Omega* 2021, 6, 25782−25790

Read Online

ACCESS | Metrics & More | Article Recommendations

ABSTRACT: Core−shell micro-spheres (MS) with both negative and positive charges in the core and only negative charges in the shell were developed as adaptive plugging agents for in-depth conformance control for enhanced oil recovery. The MS were designed to propagate deeply into the reservoir due to the small particle size and electrostatic repulsion between the MS and the sandstone at the initial stage of injection and form aggregates by electrostatic attraction between the cores with mixed charges when the shells degraded at a given time during transportation, leading to an effective plugging of the highly permeable layers with low residual oil saturation. The self-assembling and plugging behaviors of the MS have been studied by Monte Carlo simulation. The results show that charge density (D_{charge}), fraction of positive charge (F_p), MS concentration, temperature, and salinity are the key factors influencing the self-assembling behaviors. The electrostatic interaction would become stronger with the increase in D_{charge} when it is larger than 0.5. The MS are more likely to form aggregates when F_p approaches 0.5. The higher the concentration of the MS, the stronger the electrostatic interaction between the MS. In addition, electrostatic interactions between the MS become stronger with the increase in temperature and decrease in salinity. Simulation results prove that the MS with mixed charges can effectively and adaptively plug highly permeable layers with low residual oil saturation through self-assembling by combination of electrostatic interactions along with physical bridging, leading to the improvement of oil recovery. Furthermore, block charge distribution will be helpful for the MS with mixed charges to form larger aggregates than that of the random mode to effectively plug the highly permeable layers.

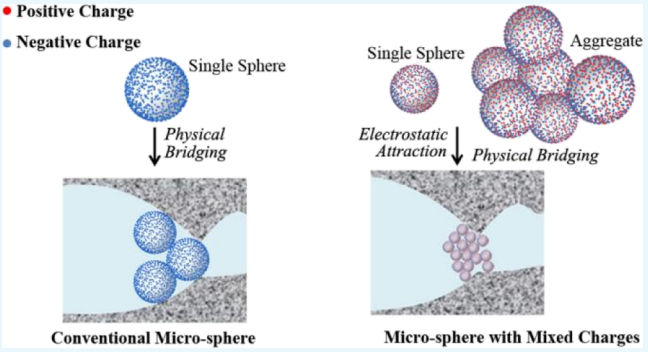

1. INTRODUCTION

More and more mature oilfields in China become seriously heterogeneous[1,2] with high water cut in the extraction fluid,[3,4] resulting in low oil production and high costs. Currently, extensive chemicals have been adopted in the oilfields for profile control to reduce the water cut and improve the oil production, including foam agents[5,6] and cross-linked polymers,[7−13] such as preformed particle gels, polyacrylamide micro-spheres (MS), and underground delayed cross-linking systems.[14−16] Plugging behavior of conventional cross-linked polymers is based on the mechanism of physical bridging at reservoir pore throats, the narrowest parts where the fluid transports, depending on the size matching relationship[17−19] between the plugging agents, which are used to plug the highly permeable zones of the reservoir by physical bridging, and the reservoir pore throats. Usually, the reservoir can be effectively plugged when the sizes of plugging agents ranged from 1/3 to 1 times of reservoir pore throats in the homogeneous reservoirs,[17,19] no matter the MS is in the small initial sizes or in the big expansion sizes.[20−22] However, it is challenging to find suitable plugging agents for heterogeneous reservoirs with poly-dispersed pore throat sizes.[23,24] Therefore, it is necessary to do more research from both practical and fundamental viewpoints to design a new adaptive plugging agent for in-depth conformance control in heterogeneous reservoirs with various permeabilities.

Core−shell MS with positively and negatively charged cores wrapped by negatively charged shells were developed recently by multi-stage emulsion or micro-emulsion polymerization with different ionic monomers,[25] aiming to form aggregates adaptively for plugging highly permeable layers by electrostatic attraction along with the conventional physical bridging, as shown in Figure 1.

The mechanism of self-assembling and plugging behavior of the MS was studied by Monte Carlo simulation in this paper.

Received: August 6, 2021
Accepted: September 15, 2021
Published: September 22, 2021

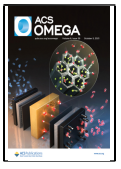

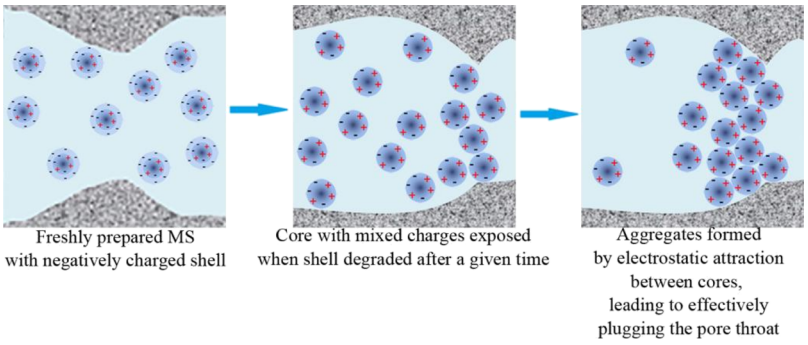

Figure 1. Scheme of the plugging process of the MS.

2. SIMULATION METHODOLOGY

Monte Carlo Simulation[26] with the canonical ensemble[27] was conducted in a two-dimensional lattice mode[28] space with either periodic or uncharged hard-wall boundary conditions. All MS moved randomly in the space. Importance sampling[29] of simulation was based on the electrostatic interaction calculated by Ewald sum adhering to Debye−Hückel theory[30] and the solvating effect described by the Flory−Huggins factor.[31]

2.1. Modeling. As hard spheres, the diameter of the MS was 24 units in the calculation cell, and each unit represented 12.5 nm in length. The MS with a diameter about 300 nm occupied 480 lattices, and each MS occupied 75 lattices on average. To simplify and speed up the simulation processes, only the MS surfaces were charged. Each lattice of the MS surface was set at most one charge by obeying the principle[32,33] that it will inhibit the ionization of the surrounding groups when one ionizable group of the polymer is ionized. Each charge on the MS surface was established as the dipole-lattice model,[34] and the length between two charges was calculated by their positions.

D_{charge} and F_p, which represented charge density and fraction of the positive charge on the MS surface, respectively, both ranged from 0 to 1. The MS surfaces were uncharged at $D_{charge} = 0$ and fully charged at $D_{charge} = 1$. There were only negative charges on the MS surface at $F_p = 0$ when D_{charge} was not zero, which could be used for representing MS wrapped by negatively charged shells. Positive and negative charges on the MS surface were distributed randomly when D_{charge} and F_p were determined except noted elsewhere. The number of charges on the surface of each MS was calculated using eq 1

$$N_{charge} = D_{charge} \cdot N_{lat\text{-}surface}$$
$$N_p = F_p \cdot N_{charge} = F_p \cdot D_{charge} \cdot N_{surface}$$
$$N_n = N_{charge} - N_p \quad (1)$$

where N_{charge} was the total number of charges, $N_{lat\text{-}surface}$ was the number of the lattice occupied by the surface of each MS, N_p was the number of positive charges, and N_n was the number of negative charges. When the results of N_{charge} and N_p were not an integer, they were round to the largest integer less than the results, respectively.

The concentration of the MS in the calculation cell, C_{ms}, was calculated using eq 2

$$C_{ms} = N_{lat\text{-}ms\text{-}total}/N_{lat\text{-}cell} = N_{ms} \cdot N_{lat\text{-}ms\text{-}one}/N_{lat\text{-}cell} \quad (2)$$

where $N_{lat\text{-}ms\text{-}total}$ was the total number of lattices occupied by all MS in the calculation cell, N_{ms} was the number of MS in the calculation cell, $N_{lat\text{-}ms\text{-}one}$ was the number of lattices occupied by one MS, and $N_{lat\text{-}cell}$ was the total number of lattices of the calculation cell. $N_{lat\text{-}cell}$ was about 4.19×10^6 by periodic boundary condition representing the MS solution with lengths of calculation cell (L_{cell}) in both horizontal and vertical direction equaled 2048 units. The hard-wall boundary condition in the vertical direction was used to represent the pore, and the vertical length (L_{cell}-y), which represented the diameter of the pore, was set to be a multiple of the MS diameter and equaled $24 \times M$, where M is the multiple of the pore size to the MS diameter. N_{cell} of the hard-wall boundary condition was $2048 \times L_{cell}$-y since the horizontal length of the calculation cell (L_{cell}-x) obtained by the periodic boundary condition remained 2048 units. The minimum number of MS for forming an entire plugging structure in the pore was defined as N_{min}. The amount of N_{min} was used to describe not only the number of MS in the pore but also the size of the aggregate which could entirely plug the pore either.

2.2. Sampling and Calculation. To estimate state Φ from state Ψ by importance sampling, the probability in simulation (P_{acc}) was expressed as eq 3[29]

$$P_{acc}(\Psi \rightarrow \Phi) = \min[c_r, \exp(-\beta \Delta E)] \quad (3)$$

where ΔE was the change in potential energy from state Ψ to state Φ, c_r was a random number ranging from 0 to 1, and β was Boltzmann constant normalized to 1 by Lennard-Jones (LJ) units, a method to set the fundamental quantities to 1 without loss of generality in simulation.

Potential energy E was separated into three independent parts: interactions between MS, interactions between MS and water, and electrostatic energy. The state change would be accepted when all three parts satisfied with the condition that the result of eq 3 was c_r.

In the hard-sphere model, the interaction energy between MS, E_{MS}, was calculated using eq 4, where $L(ij)$ was the Euclidean distance between the centers of ith and jth MS

$$E_{MS} = \begin{cases} \infty & L(ij) < 24 \\ 0 & L(ij) \geq 24 \end{cases} \quad (4)$$

Flory−Huggins factor χ, in the range of 0−1, was used to estimate the interaction between the MS and water according to eq 5[31]

$$E_{sol} = \chi \cdot Z \quad (5)$$

where E_{sol} stood for the interaction energy between MS and water and Z represented the number of lattices surrounding the MS which were occupied by the solvent. Considering that

https://doi.org/10.1021/acsomega.1c04214
ACS Omega 2021, 6, 25782−25790

the MS were highly hydrophilic in the experiment, χ was fixed at 0 in simulation.

Electrostatic energy (E_{ele}) in a lattice-mode space could be obtained using eq 6 by Fourier transform[35]

$$E_{ele} = \frac{1}{2}\sum_{i\cdot j=1}^{N_{ele}} \sum_{\mathbf{n}\in\mathbf{Z}^3} \frac{q_i q_j}{|\mathbf{r}_{ij}|\cdot\xi^*\cdot\xi_0} \tag{6}$$

where N_{ele} was the number of charges in the calculation cell, q_i and q_j ($i, j = 1 \sim N_{ele}$, $i \neq j$) represented the ith or the jth charge, respectively. ξ^* was the relative permittivity of solution, and ξ_0 was the vacuum dielectric constant. $\mathbf{r}_{ij}$ was the real space vector from ith charge with vector $\mathbf{r}_i$ to jth charge with vector $\mathbf{r}_j$.

E_{ele} would be negligibly small when $|\mathbf{r}_{ij}| > r_{max}$, and r_{max} was calculated using the Ewald parameter α,[35,36] as shown in eq 7

$$\alpha = \pi^{1/2} N_{ele}^{1/6} L_{ele}^{-1}$$
$$r_{max} \approx \pi/\alpha \tag{7}$$

where N_{ele} was the number of charge in the calculation cell and L_{ele} was the length of the calculation cell used in the calculation of E_{ele} which was 2048 with the periodic boundary condition and $(2048 \times L_{cell}\text{-}y)^{0.5}$ with the hard-wall boundary condition.

The value of N_{ele} in eq 7 was related to two parts: charges on the MS surface, which equaled $N_{ms}\cdot N_{charge}$, and ions in the solution. The number of salt ions could not be precisely set because salt ions could not been seen as a result of the high coarsening degree in simulation. Therefore, it should be unreachable to revise the data of N_{ele}, with the result that N_{ele} in eq 7 remained $N_{ms}\cdot N_{charge}$ in simulation. Besides, surface charge density and the electrical potential of the MS would be changed by salt ions,[37,38] and the influence would become stronger with higher ion concentrations. Therefore, it was necessary to revise the activity of charges on the MS surface in electrostatic energy calculation to calculate the influence of salinity in simulation considering the calculation efficiency. Assuming that there was only NaCl in the solution, the activity of surface charge, $a(S)$, was calculated using eq 8[39]

$$a(S) = 1 - \frac{S/(1000 \times 58.5)}{1 + S/(1000 \times 58.5)} \tag{8}$$

where S was the salinity of the MS solution, mg/L.

The electrical property of aqueous solution with salt ions was simulated as the continuum model[34] and was corrected by temperature (T) and salinity (S), as shown in eq 9[40]

$$\xi^*(T, S) = \xi^*(T, 0) \times (1 - 0.2551\cdot f(S) + 5.15 \times 10^{-2}\cdot f(S)^2 - 6.889 \times 10^{-3}\cdot f(S)^3) \tag{9}$$

where T was the temperature of the MS solution and $\xi^*(T, 0)$ reflected the influence of temperature on ξ^* in deionized (DI) water according to eq 10[41]

$$\xi^*(T, 0) = 87.740 - 0.4008T + 9.398 \times 10^{-4}T^{-2} - 1.410 \times 10^{-6}T^{-3} \tag{10}$$

The correction function $f(S)$ was related to the salinity of the MS solution (S, mg/L), according to the eq 11[40,42]

$$f(S) = (S/1000) \times [1.070 \times 10^{-2} + 1.205 \times 10^{-5} \times (S/1000) + 4.058 \times 10^{-9} \times (S/1000)^2] \tag{11}$$

By the normalization of ξ_0 to 1 according to LJ units, along with the correction of S and T, eq 6 would be revised to eq 12 to calculate in simulation

$$E_{ele} = \frac{1}{2}\sum_{i\cdot j=1}^{N_{ele}} \sum_{\mathbf{n}\in\mathbf{Z}^3} \frac{q_i^*\cdot q_j^*}{|\mathbf{r}_{ij}|\cdot\xi^*(T, S)}$$
$$q_i^* = q_i\cdot a(S);\ \ q_j^* = q_j\cdot a(S) \tag{12}$$

where $a(S)$ and $\xi^*(T, S)$ were obtained using eqs 8 and 9, respectively.

2.3. Statistics. To further investigate the self-assembling and motion behaviors of the MS, two series of factors, series L and series D, were considered, respectively.

Series L was based on the distribution of the MS in the calculation cell. $L(ij)$ was the Euclidean distance, as shown in eq 4. L_{ave}, L_{min}, and CV_L were the average value, the minimum value, and the coefficient variation of all $L(ij)$ in one calculation cell, respectively. With less L_{ave} or L_{min} and greater CV_L, the distribution of the MS in the calculation cell becomes more uneven, and the self-assembling behavior of MS should be more obvious.

Series D was used to estimate the motion behavior of the MS. $D(i)$ represented the contour length of the motion trajectory from the initial position to the final position of ith MS, which described the moving distance of ith MS. D_{ave} was the average value of all $D(i)$ in one calculation cell. The MS had better motility with a higher value of D_{ave}.

3. RESULTS AND DISCUSSION

3.1. Influence Factors of Self-Assembling. The influence factors of the self-assembling behaviors of the MS were studied in the MS solution using periodic boundary conditions.

3.1.1. Charge Density. The dependence of self-assembling factors on D_{charge} is shown in Figure 2.

The absolute values of E_{ele} are very small and changes little when D_{charge} is less than 0.5, implying that there is little electrostatic interaction between MS. Correspondingly, L_{ave} is almost unchanged. The absolute values of E_{ele} increase sharply with the increase in D_{charge} when D_{charge} is greater than 0.5, implying that the electrostatic interaction between MS strengthens dramatically with the increase in charge density.

At $F_p = 0$, as MS with like-charged surface repel each other, the MS separate from each other as far as possible in the limited simulation cell, leading to a disequilibrium system with $E_{ele} > 0$ at any D_{charge}, and L_{ave} reaches maximum at about $D_{charge} = 0.75$ by the limitation of the fixed concentration. The further increase in D_{charge} above 0.75 does not change the value of L_{ave} but increases the value of E_{ele} because of its non-equilibrium state.

At $F_p = 0.5$, which means the ratio of the positive charge to negative charge is 1:1 on the MS surface, E_{ele} is less than 0 at any D_{charge}. It indicates that there is electrostatic attraction between MS which dominates the self-assembling of the MS. In addition, E_{ele} increases with the increase in D_{charge}, showing that electrostatic attraction becomes stronger. Therefore the

https://doi.org/10.1021/acsomega.1c04214
ACS Omega 2021, 6, 25782−25790

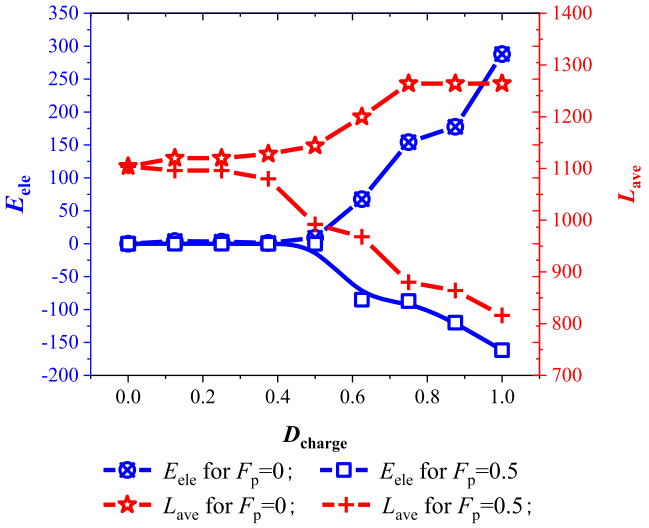

Figure 2. Dependence of E_{ele} and L_{ave} on D_{charge} at C_{ms} = 1.14 × 10^{-3} with F_p = 0 or F_p = 0.5.

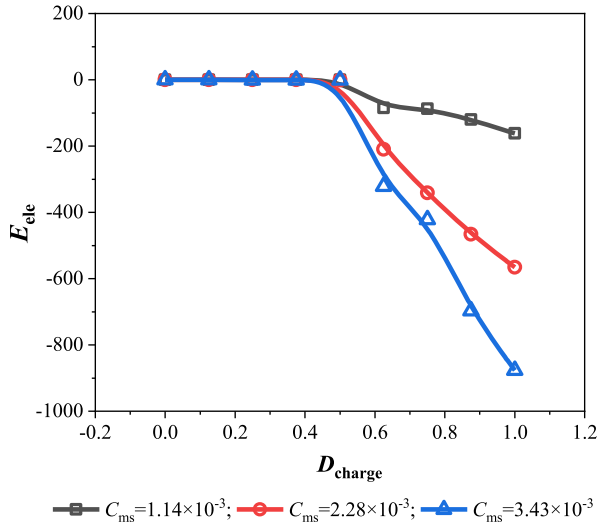

Figure 4. Dependence of E_{ele} on D_{charge} with different C_{ms} at F_p = 0.5.

MS become more inclined to assemble, resulting in the decrease in L_{ave}.

3.1.2. Fraction of Positive Charge. Figure 3 shows the dependence of self-assembling factors on F_p.

E_{ele} is below zero when F_p is between 0.3 and 0.7 and reaches the minimum at F_p = 0.5 and L_{ave}, while CV_L reaches the maximum, indicating that electrostatic attraction dominates in this range. It will lead to the self-assembling of the MS, which makes the distribution of the MS more and more uneven in the calculation cell until the number of positive charges equals to negative charges on the MS surface. The distribution of the MS varies with the change in the electrostatic interaction, depending on the value of F_p. When the fraction of either charge is below 0.3, the electrostatic repulsion will dominate the separation of the MS; hence, it is hard to form aggregates.

3.1.3. MS Concentration. Figure 4 shows the influence of charge density on E_{ele} with different MS concentrations at F_p = 0.5.

The turning points of drastic change appear at about D_{charge} = 0.5 at all concentrations, indicating that the MS concentration does not change the electrostatic properties, which are determined by the charge density on the MS surface, but only changes the absolute value of E_{ele}. The absolute value of E_{ele} becomes larger with the increase in C_{ms} at any D_{charge}, though the difference is tiny when D_{charge} < 0.5.

Figure 5 shows the influence of F_p on E_{ele} with different MS concentrations at D_{charge} = 1.

E_{ele} is less than 0 when F_p is in the range of 0.3−0.7 at any C_{ms}, and the increase in C_{ms} increases the absolute values of E_{ele}, making the self-assembling behavior of the MS more obvious when there is electrostatic attraction between MS. The attraction or repulsion between MS depends on the charge ratio on the MS surface.

3.1.4. Temperature. Figure 6 shows the dependence of ξ^* and E_{ele} on temperature (T) in DI water at D_{charge} = 1.

It is shown that ξ^* decreases with the increase in T,[41] and the absolute values of E_{ele} of MS at both F_p = 0 and F_p = 0.5 increase with the increase in T. The results for E_{ele} and ξ^* are in accordance with eq 12 which shows that E_{ele} is inversely

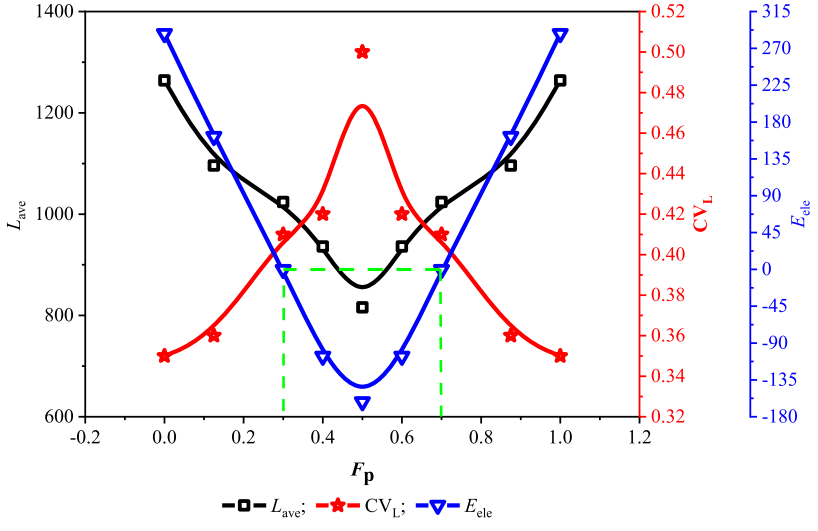

Figure 3. Dependence of self-assembling factors on F_p at D_{charge} = 1 and C_{ms} = 1.14 × 10^{-3}.

https://doi.org/10.1021/acsomega.1c04214
ACS Omega 2021, 6, 25782−25790

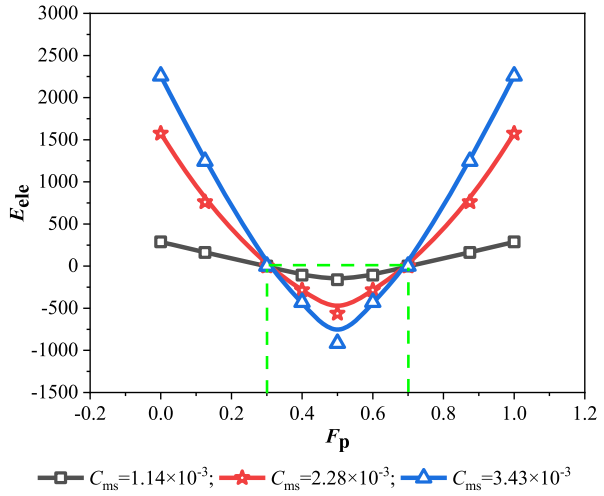

Figure 5. Dependence of E_{ele} on F_p with different C_{ms} at D_{charge} = 1.

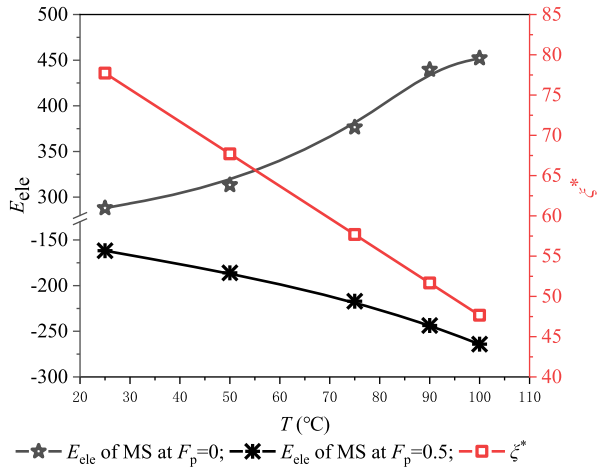

Figure 6. Dependence of ξ^* and E_{ele} on T at C_{ms} = 1.14 × 10^{-3}, S = 0 mg/L.

proportional to ξ^*. It is implied that the electrostatic interaction of either F_p enhances with the increase in T, which is helpful for the MS with mixed charges to form aggregates to plug highly permeable layers, and is crucial for enhanced oil recovery (EOR) since it is much more difficult to find suitable plugging agents for high-temperature reservoirs.[43]

3.1.5. Salinity. Since there is a wide range of salinity used in EOR, such as river water with low salinity and formation water with high salinity,[44,45] it is necessary to study the influence of salinity (S) on the electrostatic interaction and self-assembling behavior of the MS with mixed charges. Figure 7 shows ξ^*, $a(S)$, E_{ele}, and L_{ave} as functions of S at T = 95 °C and F_p = 0.5.

ξ^* and $a(S)$ decrease with the increase in S when the salinity is greater than 1000 mg/L. It has been discussed previously that E_{ele} is inversely proportional to ξ^*, but E_{ele} decreases as ξ^* decreases, as shown in Figure 7, which might be the result of the decrease in $a(S)$. $a(S)$ decreases with the increase in S, which simulates the increase in the charge shielding effect[46,47] and the decrease in the ionization possibility of charged groups on the MS surface. As a result, the absolute values of E_{ele} decrease apparently by orders of magnitude, indicating that the electrostatic attraction between MS weakens significantly with the increase in salinity, causing the decrease in self-assembling that L_{ave} grows with the increase in S, as shown in Figure 7.

3.2. Plugging Behavior of the MS in Porous Media.

The plugging behaviors of the MS were studied in porous media using hard-wall boundary conditions at D_{charge} = 1, S = 9000 mg/L, and T = 95 °C.

Figure 8 shows the minimum plugging structure in the pore. The data of N_{min} are numerically the same as M. It is found that there should be at least 1N_{min} MS in porous media to form an entire plugging structure, and C_{ms} should be higher than the critical concentration 8.78 × 10^{-3} by eq 2, otherwise the plugging behavior of the MS would not occur. Thus, the self-assembling and plugging behavior of the MS in porous media were studied when C_{ms} was higher than the critical concentration.

3.2.1. Influence of Pore Diameter on MS Size. Self-assembling behaviors of the MS in porous media at C_{ms} = 1.32 × 10^{-2} are shown in Figure 9. Though the MS concentration is higher than the critical concentration, it is still not high enough to form an aggregate for plugging.

It can been seen that the MS show the similar behaviors at F_p = 0.5 and at F_p = 0 when M equals 3, implying that physical bridging caused by geometric configuration of pores could counteract the effect of the electrostatic interaction at M = 3, no matter whatever F_p is. It is confirmed that it is the upper limit of physical bridging when the size of pore is three times that of the conventional MS.[17,19]

When the size of pores increases, MS at F_p = 0.5 could form aggregates by electrostatic attraction, while MS at F_p = 0 are likely to separate from each other and distributed in the entire space of the calculation cell. The simulation results prove that MS wrapped by negative shells could transport in the porous media.

3.2.2. Influence of the MS Concentration. To investigate the plugging behaviors of the MS at F_p = 0.5, a series of simulations have been carried out and are shown in Figure 10 with different MS concentrations.

It can be seen that even the number of the MS is larger than the least needed to form an entire plugging structure at C_{ms} = 2.20 × 10^{-2} (2.5N_{min}), which is higher than the critical concentration, it is still difficult to form at least one entire plugging structure in porous media with different sizes. However, there are some small aggregates formed which may change the flow in porous media.

When the concentration of the MS reaches 4.39 × 10^{-2} (5N_{min}), the entire plugging structures occur at M = 3 and M = 8, though they seem to be different. As highlighted by red circles in Figure 10 at C_{ms} = 4.39 × 10^{-2}, the number of MS for forming the plugging structures at M = 3 is 1N_{min}, while the number of which at M = 8 is about 1.5N_{min}.

When pore diameter increases to M = 16, 5N_{min} is not enough to form an entire plugging structure. By increasing the MS concentration to 6.59 × 10^{-2} (7.5N_{min}), an entire plugging structure occurs in the calculation cell, and the number of MS for forming the structure highlighted by red circle at C_{ms} = 6.59 × 10^{-2} is about 2N_{min}, larger than that at C_{ms} = 4.39 × 10^{-2} at M = 3 or 8. At C_{ms} = 6.59 × 10^{-2} in the small pores, more plugging structures are formed as a result of the increased number of MS at M = 3, and the size of the plugging structure at M = 8 becomes larger, as 1.5 or 2 times of which at C_{ms} = 4.39 × 10^{-2}.

The plugging behaviors, as shown in Figure 10, have proved that the MS with mixed charges could improve the upper limit of physical bridging for conventional MS, which is triple of the MS diameter,[17,19] and break through the pore throat matching

https://doi.org/10.1021/acsomega.1c04214
ACS Omega 2021, 6, 25782−25790

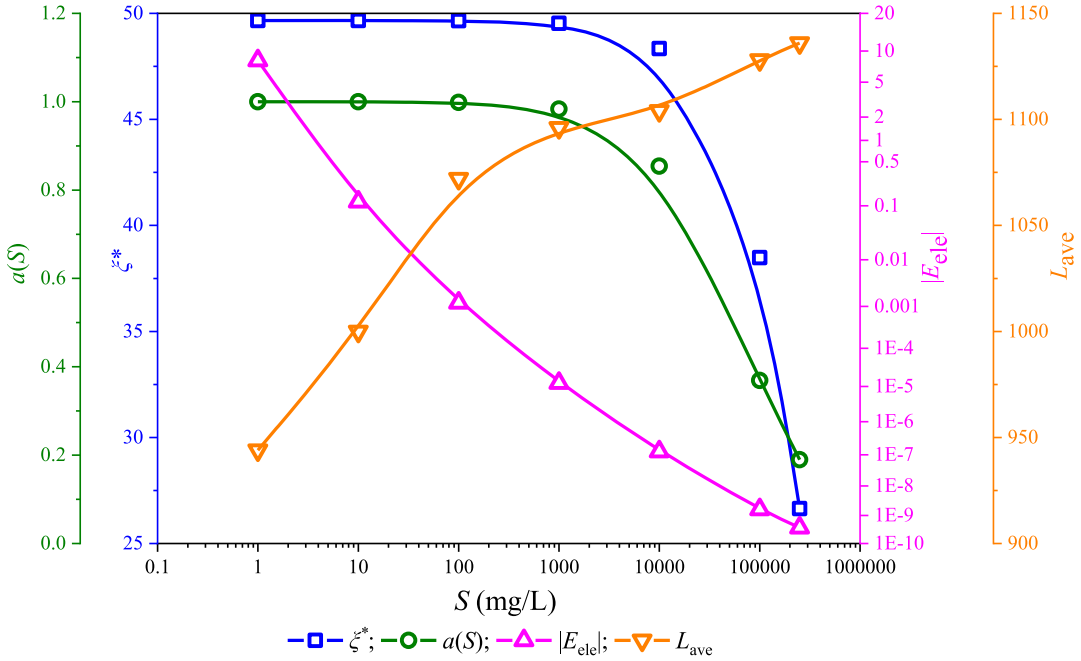

Figure 7. Dependence of ξ^*, $a(S)$, E_{ele} and L_{ave} on S at C_{ms} = 1.14 × 10^{-3}, T = 95 °C, and F_p = 0.5.

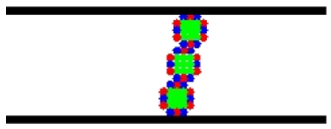

Figure 8. Scheme of the minimum plugging structure at M = 3.

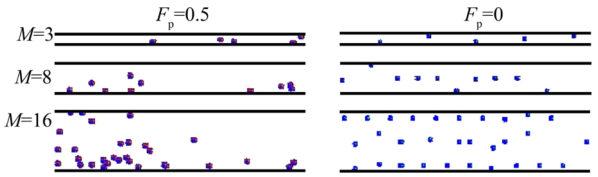

Figure 9. MS in porous media with different pore sizes at C_{ms} = 1.32 × 10^{-2}.

theory,[17−19] which can be adopted to plug larger pores by electrostatic interaction rather than physical bridging. To avoid plugging near the injection well, the MS will be wrapped by negatively charged shell to move deeply into the reservoir. Moreover, to achieve adaptive in-deep conformation control in the heterogeneous reservoir, it should be mentioned that the higher MS concentration is also important to efficiently plug high permeability reservoirs with low oil saturation.

3.3. Charge Distribution. All the discussion above are about the random distribution of charges on the MS surface, but different modes of charge distribution on the MS surface would influence the electrostatic interaction between MS. Two models of charge distribution, block mode and random mode, are discussed in this section at F_p = 0.5. Figure 11 schematically shows these two models, where positive and negative charges are drawn as red and blue spots, respectively, on the MS surface.

The most extreme block charge distribution on the MS surface is charged Janus particle,[48−50] as shown in Figure 11a that there are only two segments on the MS surface, one is positively charged, and the other is negatively charged. All charges face opposite ones on the nearby MS surface at an appropriate position when electrostatic attraction reaches its maximum, as shown in Figure 11a, which is thermodynamically favorable to induce the MS to form large aggregates. On the other hand, at a random mode, as shown in Figure 11b, it is hard to match all positive and negative segments. Consequently, electrostatic attraction could be much stronger at the block mode than that at the random mode.

The assembling behaviors of MS at F_p = 0.5 with different charge distribution modes at C_{ms} = 3.43 × 10^{-3} are shown in Figure 12.

MS at the block mode show stronger electrostatic attraction, leading to larger aggregates than that at the random mode. For the block mode, aggregates are formed by 7−10 MS. Because of the small screening length between aggregates,[48,49] the

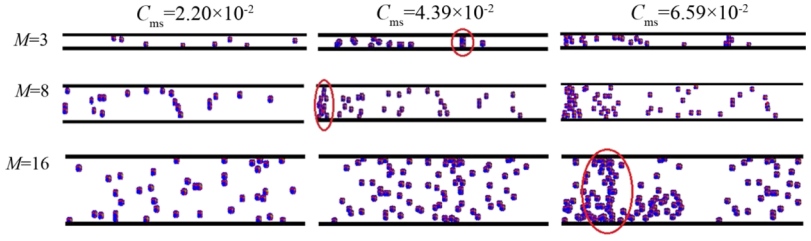

Figure 10. Self-assembling and plugging behavior of MS at F_p = 0.5 in porous media.

https://doi.org/10.1021/acsomega.1c04214
ACS Omega 2021, 6, 25782−25790

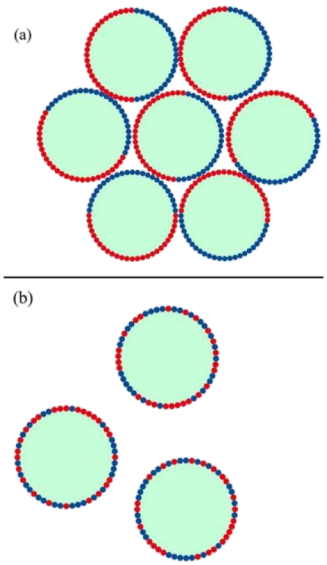

Figure 11. Scheme of different charge distribution: (a) block mode and (b) random mode ○ (red): positive charge; ○ (blue): negative charge.

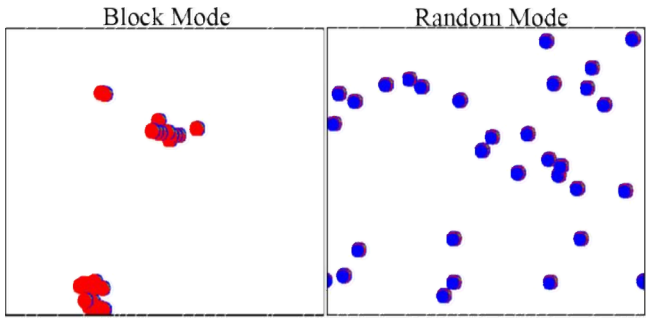

Figure 12. Self-assembling behaviors of MS at F_p = 0.5 with different charge distribution modes at C_{ms} = 3.43 × 10^{-3}.

electrostatic interaction between these aggregates is screened. Therefore, further simulation will not yield larger aggregates but the phase separation.[50] MS at the random mode are separated and distributed all over the space in the calculation cell and form small aggregates by 2−3 MS, less than that at the block mode.

All the self-assembling factors based on Figure 12 are shown in Table 1. It can be seen that L_{min} and L_{ave} at the block mode

Table 1. Self-Assembling Factors of MS at Different Charge Distribution Modes at F_p = 0.5

charge distribution	L_{ave}	L_{min}	CV_L	D_{ave}
block mode	737	24.0	0.78	66
random mode	881	65.6	0.40	19,520

are significantly less than that at the random mode, and the values of CV_L show opposite trends, which confirms that MS at the block mode are distributed more unevenly by stronger self-assembling than at the random mode.

It is shown in Table 1 that D_{ave} at the block mode is significantly less than that at the random mode. MS at the block mode are unlike to move in water solution by strong electrostatic interactions, which is at a disadvantage in simulation for its strong initial state dependence, but will be helpful for plugging the highly permeable layers for adaptable profile control and improving oil recovery because MS at the block mode would stop at a fixed point after degrading shells and form aggregates for effective plugging as the result of their less motility.

4. CONCLUSIONS

Monte Carlo simulation was used to systematically study the self-assembling and plugging behavior of core−shell MS with both negative and positive charges on the core surface and only negative charges on the shell surface.

(1) D_{charge} and F_p are the key factors in influencing the self-assembling behavior of the MS along with concentration, temperature, and salinity. The increase in D_{charge} would enhance the electrostatic interaction between the MS. Aggregates were formed when F_p was in the range of 0.3−0.7 by electrostatic attraction, and the largest aggregates were found when F_p equaled 0.5. High concentration, high temperature, and low salinity would increase the electrostatic interaction between the MS.

(2) It is confirmed that the MS with mixed charges could break through conventional size matching theory and conduct an effective plugging performance in highly permeable layers with low oil saturation by electrostatic attraction along with physical bridging for EOR.

(3) It is helpful for the MS with mixed charges to form large aggregates to plug the highly permeable layers when charges are block distributed on the MS surface.

AUTHOR INFORMATION

Corresponding Author

Yingcheng Li − *SINOPEC Shanghai Research Institute of Petrochemical Technology, Shanghai 201208, China*; Email: liyc.sshy@sinopec.com

Authors

Hui Xu − *SINOPEC Shanghai Research Institute of Petrochemical Technology, Shanghai 201208, China*; orcid.org/0000-0003-3433-540X

Zhiqing Su − *SINOPEC Shanghai Research Institute of Petrochemical Technology, Shanghai 201208, China*

Guang Yang − *SINOPEC Shanghai Research Institute of Petrochemical Technology, Shanghai 201208, China*

Xue Pu − *SINOPEC Shanghai Research Institute of Petrochemical Technology, Shanghai 201208, China*

Hui Sun − *SINOPEC Shanghai Research Institute of Petrochemical Technology, Shanghai 201208, China*

Jun Jin − *SINOPEC Shanghai Research Institute of Petrochemical Technology, Shanghai 201208, China*

Yanmin Xia − *SINOPEC Shanghai Research Institute of Petrochemical Technology, Shanghai 201208, China*

Complete contact information is available at: https://pubs.acs.org/10.1021/acsomega.1c04214

Funding

This research is supported by the China Petrochemical Corporation, and the grant number is 217007.

Notes

The authors declare no competing financial interest.

ACKNOWLEDGMENTS

We thank Kai Wang for his graphic support.

REFERENCES

(1) Xie, R. J.; Ma, Y. L.; Li, Z. Y.; Zhen, H.; Yang, Z. P. Research on reservoir heterogeneity of complex region. *Appl. Mech. Mater.* **2014**, *608−609*, 742−747.

(2) Wei, Q. L.; Xiao, L. The reservoir plane heterogeneity characteristics of the number 2 of the Shanxi formation in Changbei gas field, Ordos Basin, China. *Adv. Mater. Res.* **2012**, *524−527*, 81−84.

(3) Liu, Z.-b.; Liu, H.-h. An effective method to predict oil recovery in high water cut stage. *J. Hydrodyn.* **2015**, *27*, 988−995.

(4) Guan, C.; Hu, W.; Li, Y.; Ma, R.; Ma, Z. Prediction of oil-water relative permeability with a fractal method in ultra-high water cut stage. *J. Heat Mass Transf.* **2019**, *130*, 1045−1052.

(5) Sun, L.; Wei, P.; Pu, W.; Wang, B.; Wu, Y.; Tan, T. The oil recovery enhancement by nitrogen foam in high-temperature and high-salinity environments. *J. Petrol. Sci. Eng.* **2016**, *147*, 485−494.

(6) Clark, J. A.; Santiso, E. E. Carbon sequestration through CO_2 foam-enhanced oil recovery: A green chemistry perspective. *Engineering* **2018**, *4*, 336−342.

(7) Goudarzi, A.; Zhang, H.; Varavei, A.; Taksaudom, P.; Hu, Y.; Delshad, M.; Bai, B.; Sepehrnoori, K. A laboratory and simulation study of preformed particle gels for water conformance control. *Fuel* **2015**, *140*, 502−513.

(8) Ma, G.; Shen, Y.; Wang, X.; Guo, X.; Wu, Z. Vermiculite/polyacrylamide copolymers micro-spheres for profile control in oilfields. *J. Appl. Polym. Sci.* **2017**, *134*, 44918.

(9) Yao, C. J.; Xu, X. H.; Wang, D.; Lei, G. L.; Xue, S. J.; Hou, J.; Cathles, L. M.; Steenhuis, T. S. Research and application of micron-size polyacrylamide elastic micro-spheres as a smart sweep improvement and profile modification agent. SPE-179531-MS, presented at *SPE Improved Oil Recovery Conference*: Tulsa, Oklahoma, USA, April 11−13, 2016.

(10) Xie, G.; Luo, P.; Deng, M.; Wang, Z. Nanoplugging performance of hyperbranched polyamine as nanoplugging agent in oil-based drilling fluid. *J. Nanomater.* **2015**, *16*, 396.

(11) Cheraghian, G.; Hendraningrat, L. A review on applications of nanotechnology in the enhanced oil recovery part B: effects of nanoparticles on flooding. *Int. Nano Lett.* **2016**, *6*, 1−10.

(12) Cheraghian, G.; Hendraningrat, L. A review on applications of nanotechnology in the enhanced oil recovery part A: effects of nanoparticles on interfacial tension. *Int. Nano Lett.* **2016**, *6*, 129−138.

(13) Abdelfatah, E.; Pournik, M.; Shiau, B. J. B.; Harwell, J. Mathematical modeling and simulation of nanoparticles transport in heterogeneous porous media. *J. Nat. Gas Sci. Eng.* **2017**, *40*, 1−16.

(14) Brattekås, B.; Pedersen, S. G.; Nistov, H. T.; Haugen, Å.; Graue, A.; Liang, J.-T.; Seright, R. S. Washout of Cr(III)-Acetate-HPAM gels from fractures: Effect of gel state during placement. *SPE Prod. Oper.* **2015**, *30*, 99−109.

(15) Li, L.; Al-Muntasheri, G. A.; Liang, F. A review of crosslinked fracturing fluids prepared with produced water. *Petroleum* **2016**, *2*, 313−323.

(16) Varshney, M.; Goyal, A.; Goyal, I.; Jain, A.; Pandey, N.; Parasher, A.; Vermani, S.; Negi, A. S.; Sharma, V. Improving conformance in an injector well using delayed crosslink polymer gel : A case study. SPE-192136-MS, presented at *SPE Asia Pacific Oil and Gas Conference and Exhibition*: Brisbane, Australia, Oct 23−25, 2018.

(17) Hua, Z.; Lin, M.; Guo, J.; Xu, F.; Li, Z.; Li, M. Study on plugging performance of cross-linked polymer micro-spheres with reservoir pores. *J. Petrol. Sci. Eng.* **2013**, *105*, 70−75.

(18) Tang, X.; Yang, H.; Gao, Y.; Lashari, Z. A.; Cao, C.; Kang, W. Preparation of a micron-size silica-reinforced polymer microsphere and evaluation of its properties as a plugging agent. *Colloids Surf., A* **2018**, *547*, 8−18.

(19) Lin, M.; Zhang, G.; Hua, Z.; Zhao, Q.; Sun, F. Conformation and plugging properties of crosslinked polymer micro-spheres for profile control. *Colloids Surf., A* **2015**, *477*, 49−54.

(20) Li, J.; Niu, L.; Lu, X. Migration characteristics and deep profile control mechanism of polymer microspheres in porous media. *Energy Sci. Eng.* **2019**, *7*, 2026−2045.

(21) Tian, Q.; Wang, L.; Tang, Y.; Liu, C.; Ma, C.; Wang, T. Research and application of nano polymer microspheres diversion technique of deep fluid. SPE-156999-MS, presented at the *SPE International Oilfield Nanotechnology Conference and Exhibition*: Noordwijk, The Netherlands, June 12−14, 2012.

(22) Yu, Q.; Lu, X.; Jin, Y.; Zhang, C.; Liu, K.; Hu, X. Preparation and characterization of hydrophobic-associated microspheres for deep profile control in offshore oilfields. *Int. J. Polym. Sci.* **2018**, *2018*, 6362518.

(23) Aminian, K.; Ameri, S.; Bilgesu, H. I.; Alla, V.; Mustafa, R. Characterization of a heterogeneous reservoir in west virginia. SPE-84830-MS, presented at *SPE Eastern Regional Meeting*: Pittsburgh, Pennsylvania, USA, Sept 6−10, 2003.

(24) Afra, S.; Gildin, E.; Tarrahi, M. Heterogeneous reservoir characterization using efficient parameterization through higher order SVD (HOSVD). 14481152, presented at *IEEE 2014 American Control Conference*: Portland, Oregon, USA, June 4−6, 2014.

(25) Xia, Y.; Su, Z.; Xu, H.; Sa, O. Polyacrylamide micro-spheres as plugging agent: polymerization method and application. CN 108315003 B, PRC 201710033714.6, Jan 17, 2017.

(26) Rosenbluth, M. N.; Rosenbluth, A. W. Monte Carlo calculation of the average extension of molecular chains. *J. Chem. Phys.* **1955**, *23*, 356−359.

(27) Nosé, S. A unified formulation of the constant temperature molecular dynamics methods. *J. Chem. Phys.* **1984**, *81*, 511−519.

(28) Genzel, L.; Renk, K. F.; Weber, R. Calculation of the impurity-induced lattice mode absorption. *Phys. Status Solidi B* **1965**, *12*, 639−648.

(29) Metropolis, N.; Rosenbluth, A. W.; Rosenbluth, M. N.; Teller, A. H.; Teller, E. Equation of state calculations by fast computing machines. *J. Chem. Phys.* **1953**, *21*, 1087−1092.

(30) Ewald, P. P. Die Berechnung optischer und elektrostatischer Gitterpotentiale. *Ann. Phys.* **1921**, *369*, 253−287.

(31) Flory, P. J. Thermodynamics of high polymer solutions. *J. Chem. Phys.* **1942**, *10*, 51−61.

(32) Borkovec, M.; Daicicb, J.; Koper, G. J. M. Ionization properties of interfaces and linear polyelectrolytes: a discrete charge Ising model. *Physica A* **2001**, *298*, 1−23.

(33) Koper, G. J. M.; Borkovec, M. Proton binding by linear, branched, and hyperbranched polyelectrolytes. *Polymer* **2010**, *51*, 5649−5662.

(34) Warshel, A.; Papazyan, A. Electrostatic effects in macromolecules: fundamental concepts and practical modeling. *Struct. Biol.* **1998**, *8*, 211−217.

(35) Deserno, M.; Holm, C. How to mesh up Ewald sums. I. A theoretical and numerical comparison of various particle mesh routines. *J. Chem. Phys.* **1998**, *109*, 7678−7693.

(36) Deserno, M.; Holm, C. How to mesh up Ewald sums. II. An accurate error estimate for the particle-particle-particle - mesh algorithm. *J. Chem. Phys.* **1998**, *109*, 7694−7701.

(37) Kant, R.; Singh, M. B. Generalization of the Gouy-Chapman-Stern model of an electric double layer for a morphologically complex electrode: Deterministic and stochastic morphologies. *Phys. Rev. E: Stat., Nonlinear, Soft Matter Phys.* **2013**, *88*, 052303.

(38) Stern, O. The theory of the electrolytic double shift. *Z. Elektrochem. Angew. Phys. Chem.* **1924**, *30*, 508−516.

(39) Kim, J. H.; Yoon, J. Y. Protein adsorption on polymer particles. In *Book: Encyclopedia of Surface and Colloid Science*; Marcel Dekker Inc.: Nueva York, 2002; p 4373.

(40) Hasted, J. B.; Ritson, D. M.; Collie, C. H. Dielectric properties of aqueous ionic solutions Parts I and II. *J. Chem. Phys.* **1948**, *16*, 1.

(41) Malmberg, C. G.; Maryott, A. A. Dielectric constant of water from 0°C to 100°C. *J. Res. Natl. Bur. Stand.* **1956**, *56*, 2641−2648.

(42) Stogryn, A. Equations for calculating the dielectric constant of saline water (Correspondence). *IEEE Trans. MTT.* **1971**, *19*, 733−736.

(43) Yuan, C.-D.; Pu, W.-F.; Jin, F.-Y.; Zhang, Y.-C.; Jia, H.; Zhao, T.-h. Performance of oil-based cement slurry as a selective water-

https://doi.org/10.1021/acsomega.1c04214
ACS Omega 2021, 6, 25782−25790

plugging agent in high-temperature and high-salinity cave-fractured carbonate reservoirs. *Ind. Eng. Chem. Res.* **2014**, *53*, 6137−6149.
(44) Feng, C. *Origin of formation water salinity variation and its geological significance in Chang 9 Stratum, Jiyuan Oilfield, China, presented at European Regional Conference and Exhibition*: Lisbon, Portugal, May 18, 2015.
(45) Xie, X.; Jiu, J. J.; Li, S.; Cheng, J. Salinity variation of formation water and diagenesis reaction in abnormal pressure environments. *Sci. China, Ser. D: Earth Sci.* **2003**, *46*, 269−284.
(46) Becker, A. L.; Henzler, K.; Welsch, N.; Ballauff, M.; Borisov, O. Proteins and polyelectrolytes: A charged relationship. *Curr. Opin. Colloid Interface Sci.* **2012**, *17*, 90−96.
(47) Moerz, S. T.; Huber, P. Protein adsorption into mesopores: A combination of electrostatic interaction, counterion release, and van der Waals Forces. *Langmuir* **2014**, *30*, 2729−2737.
(48) Hu, D. M.; Cao, Q. Q.; Zuo, C. C. Effect of charge distribution on the electrostatic adsorption of Janus nanoparticles onto charged surface. *AIP Adv.* **2017**, *7*, 035006.
(49) Hieronimus, R.; Raschke, S.; Heuer, A. How to model the interaction of charged Janus particles. *J. Chem. Phys.* **2016**, *145*, 064303.
(50) Pu, M.; Jiang, H.; Hou, Z. Reentrant phase separation behavior of active particles with anisotropic Janus interaction. *Soft Matter* **2017**, *13*, 4112−4121.

https://doi.org/10.1021/acsomega.1c04214
ACS Omega 2021, 6, 25782−25790